sp-d Exchange Interactions in Wave Function Engineered Colloidal CdSe/Mn:CdS Hetero-Nanoplatelets

Franziska Muckel,[†,‡] Savas Delikanli,[§,‡] Pedro Ludwig Hernández-Martínez,[§,#] Tamara Priesner,[†] Severin Lorenz, [†] Julia Ackermann,[†] Manoj Sharma, [§,#] Hilmi Volkan Demir,[§,#,] and Gerd Bacher[†,*]*

[†]Werkstoffe der Elektrotechnik and CENIDE, University Duisburg-Essen, Bismarckstraße 81, 47057 Duisburg, Germany

[§]LUMINOUS! Center of Excellence for Semiconductor Lighting and Displays, School of Electrical and Electronic Engineering, School of Physical and Materials Sciences, School of Materials Sciences and Engineering, Nanyang Technological University, Singapore 639798

[#]Department of Electrical and Electronics Engineering, Department of Physics, UNAM - Institute of Materials Science and Nanotechnology, Bilkent University, Ankara 06800, Turkey

In two-dimensional (2D) colloidal semiconductor nanoplatelets, which are atomically flat nanocrystals, the precise control of thickness and composition on the atomic scale allows for the synthesis of heterostructures with well-defined electron and hole wave function distributions. Introducing transition metal dopants with monolayer precision enables tailored magnetic exchange interactions between dopants and band states. Here, we use the absorption based technique of magnetic circular dichroism (MCD) to directly prove exchange coupling of magnetic dopants with the band charge carriers in shell-doped CdSe/Mn:CdS hetero-nanoplatelets. We show that the strength of both the electron as well as the hole exchange interactions with the dopants can be tuned by varying the nanoplatelets architecture with monolayer accuracy. As MCD is highly sensitive for excitonic resonances, excited level spectroscopy allows us to resolve and identify - in combination with wave function calculations - several excited state transitions including spin-orbit split-off excitonic contributions. Thus, our study not only demonstrates the possibility to expand the extraordinary physical properties of colloidal nanoplatelets towards magneto-optical functionality by transition metal doping, but in addition provides an insight to the excited state electronic structure in this novel two-dimensional materials.

Keywords: colloidal nanoplatelets, colloidal heterostructures, semiconductor nanocrystals, wave function engineering, transition metal doping, magnetic circular dichroism (MCD), diluted magnetic semiconductor (DMS)

Recently novel two-dimensional (2D) colloidal nanoplatelets (NPLs), the so-called 'colloidal quantum wells', evoke increasing research interest as functional materials in next-generation optoelectronic and photonic devices, such as light-emitting diodes[1,2] and lasing applications,[3–5] thanks to their outstanding electronic and optical properties.[6–8] These semiconductor nanocrystals, which are precisely tunable in thickness on a monolayer scale, combine short fluorescence lifetimes and high ensemble color purities[9] with a distinct 2D electronic structure,[10] large absorption cross-sections[11] and quasi-zero Stokes's shift. The lately developed technique of colloidal atomic layer deposition (c-ALD)[12] allows the synthesis of complex core/shell heterostructure architectures. This opens up access to various material combinations enabling precise tuning of the band alignment and thus the charge carrier wave functions in, e.g., type I[13], quasi-type II[14,15] and type II[16,17] heterojunctions.

Doping - the selective introduction of impurity atoms on lattice sites - represents a powerful approach to tailor the optical, electrical and magnetic properties of a semiconductor and has successfully been adapted in various colloidal nanocrystals.[18–22] Embedding transition metal ions like manganese into semiconductors is known to introduce magnetic *sp-d* exchange interactions between the magnetic moments of the dopants (carried by their *d* orbitals) and the spins of the charge carriers, i.e., the (*s*-type) electrons and the (*p*-type) holes, which results in extraordinary optical and magneto-optical properties.[23,24] This concept of diluted magnetic semiconductors (DMS) experiences a boost since its adaption to colloidal synthesized nanocrystals,[19,25,26] as herein the magnetic exchange interactions - scaling with the wave function overlap of the charge carriers with the dopants - can be greatly enhanced due to the strong geometrical and dielectric confinement achievable in comparison to their epitaxial counterparts. This has led to, e.g., the

observation of giant zero field exchange splitting in single-Mn-doped CdSe quantum dots (QDs)[27] and light induced magnetism up to room temperature in Mn:CdSe QDs[28] – making colloidal DMS nanostructures attractive for the incorporation in tomorrow's spintronic devices.[29] In various magnetically doped colloidal nanostructures of different shapes (including spherical quantum dots,[30] magic sized clusters[31] and anisotropic nanoribbons[32]) *sp-d* exchange interactions persist up to room temperature.

Very recently magnetic doping has been realized in CdSe/Mn:CdS/CdS multishell nanoplatelets,[33,34] extending the versatile outstanding properties of NPLs towards magneto-optical functionality. The distinct two-dimensional electronic structure allows one to selectively address individual excitonic transitions with well-defined hole character. This is in contrast to spherical magnetically doped core/shell quantum dots[35,36], which are strongly affected by valance band mixing.

In this work, we utilize magnetic circular dichroism (MCD) spectroscopy to directly evidence *sp-d* exchange interactions in shell-doped CdSe(/MnS)/Mn:CdS core/shell nanoplatelets. By exploring the degrees of freedom provided by c-ALD, we show the possibility to tune the *s-d* and *p-d* exchange interactions via wave function engineering. By variation of the core and shell thickness in CdSe/Mn:CdS nanoplatelets with atomic monolayer precision we are able to adjust the *p-d* exchange interactions. Integration of a high-bandgap MnS interlayer enables us to confine the heavy hole wave function in the undoped core, giving access to tune the *s-d* exchange interactions. Excited state MCD spectroscopy reveals a variety of excitonic resonances. They could be successfully identified and assigned via wave function calculations, providing valuable insights into the excited states electronic structure of this novel class of materials.

Magnetically doped nanoplatelets of zinc blende type were synthesized following the synthesis described in Ref. [33]. For our study we prepared two sets of samples allowing us to tune either the hole (*p-d*) or the electron (*s-d*) exchange interaction with magnetic dopants. For studying the former (i.e., the *p-d* exchange interaction), an undoped CdSe core of 2 or 3 monolayer (ML) thickness was coated with a manganese-doped shell of 6 or 8 ML thickness (3 or 4 ML on each side, respectively). In order to tune the *s-d* exchange interaction, we prepared samples based on a 2 ML CdSe core surrounded by a 2 ML (one on each side) MnS interlayer and additional 6 to 10 ML (3 to 5 on each side) Mn:CdS. The doping concentration in the Mn:CdS shell is approximately 1.2% (see Supporting Information). A list of all doped samples can be found in Table 1.

Table 1. List of samples used in this study.

Samples	**Composition**		
	CdSe core	*MnS* interlayer	*Mn:CdS* shell
(2) CdSe / (8) Mn:CdS	2 ML	-	2 × 4 ML
(2) CdSe / (6) Mn:CdS	2 ML	-	2 × 3 ML
(3) CdSe / (8) Mn:CdS	3 ML	-	2 × 4 ML
(2) CdSe / (2) MnS / (6) Mn:CdS	2 ML	2 × 1 ML	2 × 3 ML
(2) CdSe / (2) MnS / (8) Mn:CdS	2 ML	2 × 1 ML	2 × 4 ML
(2) CdSe / (2) MnS / (10) Mn:CdS	2 ML	2 × 1 ML	2 × 5 ML

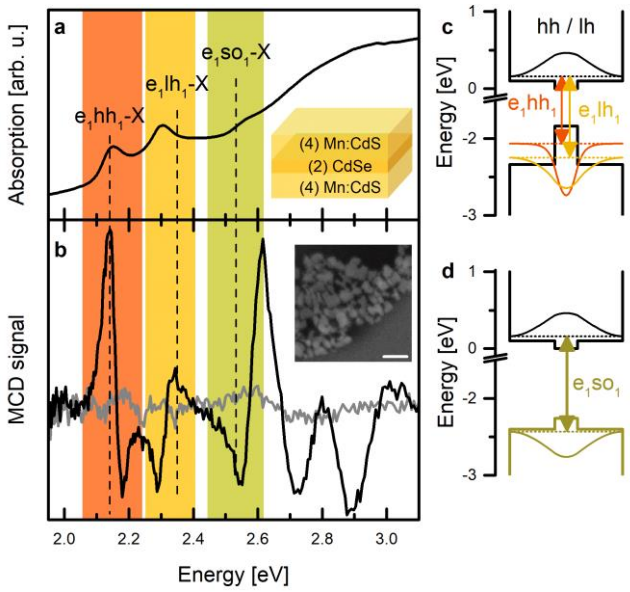

Figure 1. Absorption (a) and MCD spectra (b) of (2) CdSe / (8) Mn:CdS (black) nanoplatelets at 5 K and under 1.6 T. For comparison, the magneto-optical response of an undoped reference (gray line) with the same architecture ((2) CdSe / (8) CdS) is depicted. The spectral range of the e_1hh_1-X, e_1lh_1-X and e_1so_1-X transitions are highlighted in red, yellow and olive, respectively, while dashed lines represent the calculated transition energies considering exciton binding energies (see Supporting Information for details). The insets depict a scheme of the sample (top) and a SEM image of nanoplatelets deposited on a Si substrate (bottom, scale bar 50 nm). (c) and (d) depict calculated energies and probability density functions for the e_1 electron (black) and the hh_1 (orange), lh_1 (yellow) and so_1 (olive) hole states. Arrows denote the respective optical transitions.

Figure 1b compares the MCD signal from (2) CdSe / (8) Mn:CdS NPLs with data from an undoped reference sample at 1.6 T and cryogenic temperatures, revealing a bunch of excitonic signatures for the doped sample. Typically, an A-type MCD feature has a deviated-Gaussian line shape, with its zero crossing coinciding with the peak position in zero-field absorption, while the

sign of the corresponding Zeeman splitting is revealed in the shape of the signal (for a positive Zeeman splitting a maximum follows a minimum in energy and vice versa, following the convention of [26,37]). Comparing MCD and absorption spectra (Figure 1a), the first two energetically lowest transitions can be directly assigned to the first heavy and light hole excitonic transitions (e_1hh_1-X and e_1lh_1-X, respectively), as they coincide with the prominent absorption features commonly observed in literature.[10,38] These assignments were confirmed with double-potential quantum well calculations (Figure 1c), neglecting in a first approximation non-parabolicity effects and coupling between different states (see Supporting information for calculative details and all parameters involved). The calculated transition energies (shown in Figure 1 as dashed lines) nicely resemble the experimental data. The Zeeman splitting can be extracted according to Ref. [26] and is at B = 1.6 T in the range of -1 ± 0.5 meV for the e_1hh_1-X, thus comparable to the previously observed Zeeman splitting in shell-doped multilayer nanoplatelets with similar architecture.[33] The ratio between the e_1hh_1-X and the e_1lh_1-X splitting was determined to be $\frac{\Delta E_{lh}}{\Delta E_{hh}} = -0.54 \pm 0.08$. Based on our calculations (compare Figure 1d) we assign the third resonance at 2.57 eV to the first spin-orbit split-off exciton (e_1so_1-X) transition.

For various zinc blende bulk DMS materials it is known that the hh excitonic transition splits according to

$$\Delta E_{hh} = x_{eff}\langle S_z\rangle(\gamma_{hh}N_0\beta - \gamma_e N_0\alpha) \qquad (1)$$

with $N_0\alpha$ and $N_0\beta$ representing the electron and hole exchange coupling constants, x_{eff} the concentration of paramagnetic active Mn dopants, $\gamma_{e/hh}$ the wave function overlap between the charge carriers and the Mn ensemble and $\langle S_z\rangle$ the Mn spin expectation value.[23,24] Since the values of the exchange coupling constants usually have different signs ($N_0\alpha = 0.22$ eV and $N_0\beta = -1.8\ eV$ for Mn:CdS)[23], the giant Zeeman splitting of the e_1hh_1-X is always negative and

maximal in amplitude. This relation remains valid in quantum wells as long as both the quantization axis and the direction of the external magnetic field are parallel and point in the direction of light propagation[23,39]. This is the case in our experiment with the majority of the nanoplatelets being oriented parallel to the substrate (as apparent from the inset of Figure 1). The expected sign of the Zeeman splitting is in accordance with our experiment exhibiting a negative splitting for the e_1hh_1-X transition.

The e_1lh_1-X and e_1so_1-X transitions in zinc blende bulk DMS materials are known to split according to $\Delta E_{lh} = x_{eff}\langle S_z\rangle\left(\gamma_e N_0\alpha + \gamma_{lh}\frac{N_0\beta}{3}\right)$ and $\Delta E_{so} = x_{eff}\langle S_z\rangle\left(\gamma_e N_0\alpha - \gamma_{so}\frac{N_0\beta}{3}\right)$, respectively.[24] As for the e_1so_1-X the electron and hole contribution to the Zeeman splitting both have a positive sign, the e_1so_1-X is expected to consistently exhibit an opposite sign as compared to the e_1hh_1-X even in anisotropic systems.[40,41] The positive splitting of the third transition (at around 2.57 eV) observed in our experiments thus represents a strong indication for the assignment as e_1so_1-X. In the case of e_1lh_1-X, both exchange components compensate each other in great part,[23,24] leading to a small negative splitting in cubic bulk DMS, [42–44] which can be inverted in sign in materials with anisotropic perturbations like, e.g., a wurtzite lattice,[40,45] strain[46] and quantization.[32] Hence, the observed positive splitting of the e_1lh_1-X transition in the nanoplatelets might be due to the influence of the strong quantization combined with strain in the nominally zinc blende structured Mn:CdS shell. For excited state transitions, we accordingly expect any transition with positive splitting (i.e., a minimum followed by a maximum in MCD) to involve either an lh or a so hole state, while transitions involving an excited hh state should be characterized by a negative splitting.

As the MCD signal is highly sensitive to excitonic features,[47] it reveals a bunch of distinct transitions above 2.6 eV. These features cannot be identified in the absorption spectrum, as it

represents a superposition of excitonic transitions with inter sub-band transitions of free electrons and holes and a scattering background. Thus, through the MCD signal, magnetic doping provides a unique path to resolve the upper excitonic transitions in the 2D quantum well. The whole MCD spectrum up to 3.1 eV can be reproduced with two additional higher excitonic transitions (compare Figure S2) at 2.68 eV and 2.93 eV, respectively, which can be related to excited hole states. As discussed in the Supporting Information, we hypothesize the former to be correlated with the e_1hh_3-X, while the latter transition cannot be assigned definitely. Similar assignments (e_1hh_1-X, e_1lh_1-X and e_1hh_3-X) have been drawn in epitaxial CdMnTe quantum wells.[39]

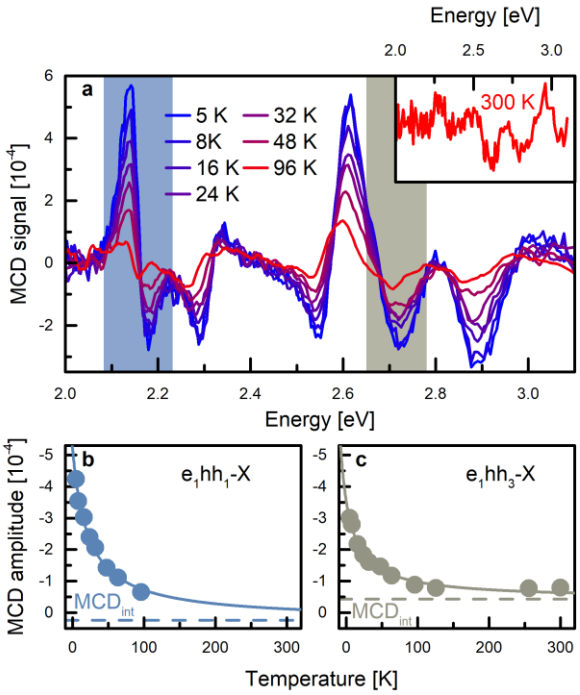

Figure 2. (a) Temperature dependence of the MCD spectra at 1.6 T between 5 and 96 K. The inset depicts the room temperature MCD signal. The spectral range of the e_1hh_1-X and the e_1hh_3-X transition are highlighted in blue and grey, respectively. (b) and (c) illustrate the decay of the MCD amplitude with temperature for both transitions highlighted in (a) (for the e_1hh_1-X the mean amplitude between the minimum and the maximum of the resonance is shown, while in the case of the e_1hh_3-X transition, which overlaps with the e_1so_1-X feature on the low energy side,

the amplitude of the minimum at 2.7 eV is taken). Dots depict the data while lines represent the Brillouin fits according to $MCD = MCD_{max} \cdot B_S(a) + MCD_{int}$. Herein, MCD_{max} denotes the maximum MCD amplitude in case that all Mn^{2+} ions are aligned along the external magnetic field, $B_s(a)$ the Brillouin function with S = 5/2 and MCD_{int} the MCD amplitude according to the internal Zeeman effect (see Supporting Information for details).

The temperature dependence of the MCD signal gives additional evidence for the *sp-d* exchange interaction as origin of the magneto-optical response. This allows distinguishing between *sp-d* exchange and intrinsic contributions to the magneto-optical response. In general, the MCD signal is composed of contributions from the *sp-d* exchange interaction and the intrinsic Zeeman splitting present in any semiconductor ($MCD = MCD_{sp-d} + MCD_{int}$). Since the MCD amplitude corresponding to the *sp-d* exchange interaction scales with the magnetization of the Mn sub-lattice given by the competition between the alignment along the external magnetic field and the disordering by the thermal energy, it declines with increasing temperature following a characteristic Brillouin function. Figures 2b and c depict the decrease of the MCD amplitude with temperature for the band edge e_1hh_1-X transition as well as for the e_1hh_3-X transition (note that the sign of the amplitude is chosen in order to correspond to the sign of the Zeeman splitting). Both data sets can be described with the same Brillouin function (and different amplitudes for the *sp-d* and the intrinsic contribution, see Supporting Information for details), which reinforces that the *sp-d* exchange interaction largely dominates the magneto-optical response for all transitions at low temperatures ($\left|\frac{MCD_{int}}{MCD}\right| < 17\%$ at 5 K for both transitions).

Interestingly, the signal of the transitions involving n = 1 hole states vanishes below the signal-to-noise-ratio at about 100 K, while the signal of the transitions involving excited hole states persists up to room temperature (compare inset in Figure 2a). This difference is related to different signs of the intrinsic MCD contribution, being positive for the ground state transitions (where the hole is mainly located in the CdSe core) while it is negative for the excited hole states, where the hole wave function strongly extends into the Mn:CdS barrier. It is known that in CdSe the intrinsic splitting owns the opposite sign compared to the giant Zeeman splitting (i.e., has a positive g-factor with g_{int} between 1.0 and 1.4[48]), while it has a negative sign in CdS ($g_{int} \approx -1.0 - 1.3$, estimated from ref. [49]). In our structure we expect contributions from both materials according to the wave function distribution between the core and the shell. As the observed ground and excited state transitions share the same e_1 electron state, the difference in the intrinsic g-factor between both excitonic transitions is related to the redistribution of the hole, which can be calculated to increase from a probability density of 0.24 in the shell for the hh_1 state to 0.93 for the hh_3 state.

Based on the assignment of the different transitions, we demonstrate exchange coupling engineering by tuning the nanoplatelets architecture exploiting the synthetic degrees of freedom provided by c-ALD. In the first series, we concentrate on the manipulation of the hole exchange coupling by changing (i) the shell thickness from 8 ML to 6 ML and (ii) the core thickness from 2 to 3 ML (compare room temperature absorbance in Figure 3a). Figure 3b illustrates the effect of a decreased shell thickness, shifting the excited hole transitions to higher energies (see MCD spectra for energies above 2.6 eV), while the ground hole states are neither affected in the energetic position nor in the MCD amplitude (see MCD spectra for energies below 2.5 eV). These observations are reflected in our calculations, as depicted in Figure 3d. While the ground

heavy hole states is not shifting at all, the excited states shift towards higher energies with decreasing shell thickness. Extracting the wave function overlap with the doped shell reveals a change of less than 15 % for the hh_1 state with varying shell thickness, while the wave function overlap γ_{so} of the so_1 state significantly decreases with decreasing shell thickness. This is summarized in Figure 3f, and is in good agreement with our experimental findings (Figure 3b).

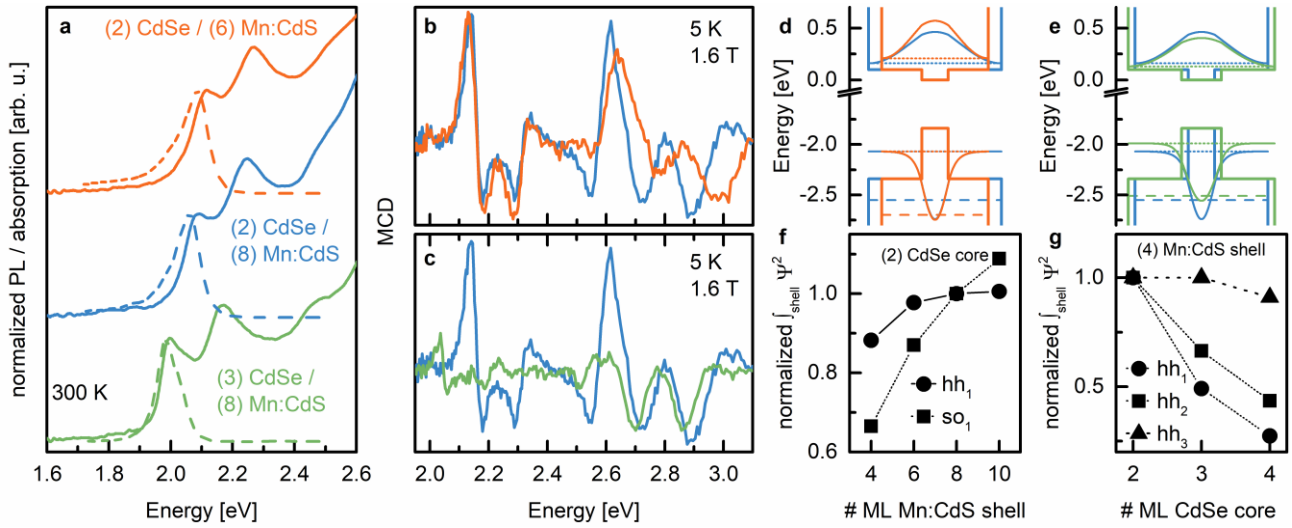

Figure 3. (a) Normalized room temperature PL (dashed lines) and absorption (solid lines) spectra of magnetically doped core-shell nanoplatelets with different core and shell thicknesses: (3) CdSe / (8) Mn:CdS nanoplatelets in green, (2) CdSe / (8) Mn:CdS nanoplatelets in blue and (2) CdSe / (6) Mn:CdS nanoplatelets in light red, respectively. (b,c) MCD signals at 5 K and 1.6 T of samples with different numbers of ML in the shell ((b), 6 ML compared to 8 ML) and different core thicknesses ((c), 2 ML vs. 3 ML). (d,e) Calculated energies of the lowest electron state e_1 in the conduction band (CB) and the hh_1 and hh_3 states in the valence band (VB), respectively. Narrow-dotted lines represent the ground states (n=1), dashed lines the n=3 states. Straight lines represent the probability density function of the electron and the heavy hole in the

n=1 state, respectively. Coloring in panels (b-e) is the same as in panel (a). (f,g) depict the integrated probability densities of selected hole wave functions in the doped shell for (f) different shell thicknesses surrounding a 2 ML CdSe core and (g) different core thicknesses with 8 ML Mn:CdS shell. All values are normalized with respect to the value in the (2) CdSe / (8) Mn:CdS sample.

Modifying the core thickness on the other hand significantly influences the excitonic transitions involving the ground hole states (compare Figure 3c): While the transitions involving excited hole states slightly shift in energy but retain their magneto-optical activity, the MCD amplitude significantly decreases for the transitions involving n=1 hole states as the core thickness is increased. Wave function calculations (compare Figure 3e) reveal that this is due to the decreasing hole wave function overlap with the doped shell, when increasing the undoped core thickness from 2 to 3 ML (e.g., γ_{hh} decreases by a factor of 2 from 0.24 to 0.12). The wave functions of the excited n=3 hole state, widely delocalized over the whole nanoplatelets thickness, is not affected to the same degree (compare Figure 3g). Changes in the core thickness do only result in a minor variation of the MCD amplitude of excitonic transition involving excited hole states. Thus, we can tune the exchange coupling between magnetic dopants and ground or excited hole states by changing either the core or the shell thickness in these hetero-nanoplatelets.

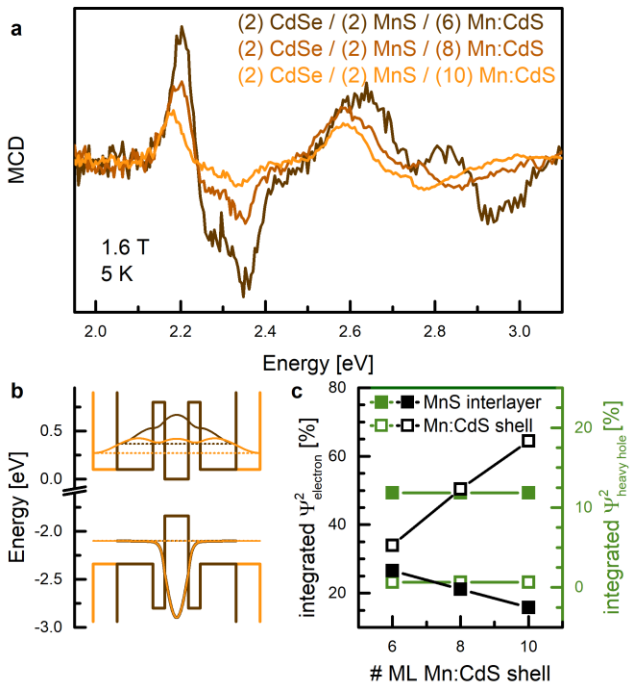

Figure 4. (a) MCD signal of nanoplatelets with 2 ML CdSe core, 2 ML (one on each side) MnS interlayer and 6 to 10 ML (3 to 5 ML on each side) Mn:CdS shell at 1.6 T and 5 K. (b) Energy states and probability density functions calculated for samples with 2 ML CdSe core, 2 ML MnS interlayer and 6 (dark brown) or 10 (orange) ML Mn:CdS shell, respectively. (c) Overlap of the electron and hole wave functions with the doped regions in the MnS interlayer and the Mn:CdS shell, respectively.

To tune the electron exchange interactions of the e_1hh_1-X, we modified the architecture of the hetero-nanoplatelets by including an additional MnS interlayer between core and shell. The MnS band gap can be extrapolated from CdMnSe to be as high as 3.6 eV at cryogenic temperatures.[50] This interlayer is thus able to confine the heavy hole wave function in the core. As the MnS layer is only a monolayer thick one each side and epitaxially grown onto the CdSe core, we expect it to have zincblende structure. Bulk zincblende β-MnS is a metastable salt, exhibiting

antiferromagnetic ordering below the Neel temperature (approximately 100 K).[51] As shown in Figure 4a, the amplitude of the MCD signal decreases among different samples with the same dimension of the core and the interlayer (2 ML CdSe, 2 ML MnS, i.e., 1 ML on each side of the core) but increasing shell thickness. Wave function calculations (compare Figure 4b) reveal that by increasing the Mn:CdS shell thickness between 6 and 10 ML we can purposely change the electron wave function distribution, while the heavy hole ground state is not affected at all. Calculating the wave function overlap of the electron and the heavy hole with the MnS interlayer on the one hand and with the Mn-doped CdS shell on the other hand (compare Figure 4c) reveals that with increasing shell thickness the electron wave function extends more and more into the Mn:CdS shell, while the wave function overlap with the MnS interlayer decreases. The decreasing amplitude of the magneto-optical response observed in experiment therefore suggests that the concentration of the magneto-optically active Mn ions is higher in the MnS interlayer compared to the Mn-doped CdS shell. This allows us to conclude that a large amount of Mn spins in the 1 ML thin MnS interlayer do behave paramagnetic without dominant antiferromagnetic coupling. Similar tendencies of a decreased Neel temperature has been observed in nanoscaled MnS thin films.[52] By confining the heavy hole in the core with the MnS interlayers tuning of the *s-d* electron exchange interaction by varying the thickness of the Mn:CdS shell is thus demonstrated for the e_1hh_1-X.

In conclusion, we demonstrated *sp-d* exchange interactions between electron and hole band states and magnetic dopants in core-shell CdS/(MnS)/Mn:CdS hetero-nanoplatelets. The high sensitivity of MCD spectroscopy for excitonic transitions allowed us to investigate the electronic structure of excited states in core/shell hetero-nanoplatelets. We were able to assign a bunch of higher transitions, including the e_1so_1-X exciton transition as well as exciton transitions

involving the e_1 electron ground state and excited hole states. The electron or hole exchange interactions could be tuned separately by modifying the architecture of the hetero-nanoplatelets, namely composition, core and shell thickness, and MnS interlayer. Our study not only proves the possibility to furnish chalcogenide nanoplatelets with tunable magneto-optical functionalities, but furthermore provides new insights into the electronic structure of this auspicious material class.

ASSOCIATED CONTENT

Supporting Information

Sample Synthesis, Experimental section, Data Analysis, Theoretical Section

AUTHOR INFORMATION

Corresponding Author

*Email: gerd.bacher@uni-due.de, volkan@stanfordalumni.org

Author Contributions

‡F. M. and S. D. contributed equally. The manuscript was written through contributions of all authors. All authors have given approval to the final version of the manuscript.

Acknowledgements

This research is supported by the German Research Foundation DFG under contract BA-1422 and the National Research Foundation, Prime Minister's Office, Singapore under its Investigatorship program (NRF-NRFI2016-08). HVD gratefully acknowledges TUBA.

REFERENCES

(1) Zhang, F.; Wang, S.; Wang, L.; Lin, Q.; Shen, H.; Cao, W.; Yang, C.; Wang, H.; Yu, L.; Du, Z.; Xue, J.; Li, L. S. *Nanoscale* **2016**, *8*, 12182–12188.

(2) Chen, Z.; Nadal, B.; Mahler, B.; Aubin, H.; Dubertret, B. *Adv. Funct. Mater.* **2014**, *24*, 295–302.

(3) She, C.; Fedin, I.; Dolzhnikov, D. S.; Demortière, A.; Schaller, R. D.; Pelton, M.; Talapin, D. V. *Nano Lett.* **2014**, *14* (5), 2772–2777.

(4) Guzelturk, B.; Kelestemur, Y.; Olutas, M.; Delikanli, S.; Demir, H. V. *ACS Nano* **2014**, *8* (7), 6599–6605.

(5) Grim, J. Q.; Christodoulou, S.; Di Stasio, F.; Krahne, R.; Cingolani, R.; Manna, L.; Moreels, I. *Nat. Nanotechnol.* **2014**, *9* (11), 891–895.

(6) Lhuillier, E.; Pedetti, S.; Ithurria, S.; Nadal, B.; Heuclin, H.; Dubertret, B. *Acc. Chem. Res.* **2015**, *48* (1), 22–30.

(7) Nasilowski, M.; Mahler, B.; Lhuillier, E.; Ithurria, S.; Dubertret, B. *Chem. Rev.* **2016**, *116* (18), 10934–10982.

(8) Scott, R.; Heckmann, J.; Prudnikau, A. V; Antanovich, A.; Mikhailov, A.; Owschimikow, N.; Artemyev, M.; Climente, J. I.; Woggon, U.; Grosse, N. B.; Achtstein, A. W. *Nat. Nanotechnol.* **2017**, *12* (12), 1155–1160.

(9) Ithurria, S.; Dubertret, B. *J. Am. Chem. Soc.* **2008**, *130* (49), 16504–16505.

(10) Ithurria, S.; Tessier, M. D.; Mahler, B.; Lobo, R. P. S. M.; Dubertret, B.; Efros, A. L. *Nat. Mater.* **2011**, *10* (12), 936–941.

(11) Yeltik, A.; Delikanli, S.; Olutas, M.; Kelestemur, Y.; Guzelturk, B.; Demir, H. V. *J. Phys. Chem. C* **2015**, *119* (47), 26768–26775.

(12) Ithurria, S.; Talapin, D. V. *J. Am. Chem. Soc.* **2012**, *134* (45), 18585–18590.

(13) Delikanli, S.; Guzelturk, B.; Hernández-Martínez, P. L.; Erdem, T.; Kelestemur, Y.; Olutas, M.; Akgul, M. Z.; Demir, H. V. *Adv. Funct. Mater.* **2015**, *25* (27), 4282–4289.

(14) Mahler, B.; Nadal, B.; Bouet, C.; Patriarche, G.; Dubertret, B. *J. Am. Chem. Soc.* **2012**, *134* (45), 18591–18598.

(15) Prudnikau, A.; Chuvilin, A.; Artemyev, M. *J. Am. Chem. Soc.* **2013**, *135* (39), 14476–14479.

(16) Pedetti, S.; Ithurria, S.; Heuclin, H.; Patriarche, G.; Dubertret, B. *J. Am. Chem. Soc.* **2014**, *136* (46), 16430–16438.

(17) Kelestemur, Y.; Olutas, M.; Delikanli, S.; Guzelturk, B.; Akgul, M. Z.; Demir, H. V. *J. Phys. Chem. C* **2015**, *119* (4), 2177–2185.

(18) Norris, D. J.; Efros, A. L.; Erwin, S. C. *Science* **2008**, *319* (5871), 1776–1779.

(19) Beaulac, R.; Archer, P. I.; Ochsenbein, S. T.; Gamelin, D. R. *Adv. Funct. Mater.* **2008**, *18* (24), 3873–3891.

(20) Schimpf, A. M.; Knowles, K. E.; Carroll, G. M.; Gamelin, D. R. *Acc. Chem. Res.* **2015**, *48* (7), 1929–1937.

(21) Knowles, K. E.; Hartstein, K. H.; Kilburn, T. B.; Marchioro, A.; Nelson, H. D.; Whitham, P. J.; Gamelin, D. R. *Chem. Rev.* **2016**, *116* (18), 10820–10851.

(22) Stavrinadis, A.; Konstantatos, G. *ChemPhysChem* **2016**, *17* (5), 632–644.

(23) Gaj, J.; Kossut, J. *Introduction to the physics of diluted magnetic semiconductors*; Springer: Berlin, Heidelberg, 2011.

(24) Furdyna, J. K.; Kossut, J. *Diluted Magnetic Semiconductors, Semiconductors and Semimetals Vol. 25*; Academic Press, Inc.: San Diego, 1988; Vol. 25.

(25) Norris, D. J.; Yao, N.; Charnock, F. T.; Kennedy, T. A. *Nano Lett.* **2001**, *1* (1), 3–7.

(26) Klimov, V. *Nanocrystal Quantum Dots*; CRC Press: Boca Raton, 2010.

(27) Fainblat, R.; Barrows, C. J.; Hopmann, E.; Siebeneicher, S.; Vlaskin, V. A.; Gamelin, D. R.; Bacher, G. *Nano Lett.* **2016**, *16* (10), 6371–6377.

(28) Beaulac, R.; Schneider, L.; Archer, P. I.; Bacher, G.; Gamelin, D. R. *Science* **2009**, *325* (5943), 973–976.

(29) Muckel, F.; Barrows, C. J.; Graf, A.; Schmitz, A.; Erickson, C. S.; Gamelin, D. R.; Bacher, G. *Nano Lett.* **2017**, *17* (8), 4768–4773.

(30) Vlaskin, V. A.; Barrows, C. J.; Erickson, C. S.; Gamelin, D. R. *J. Am. Chem. Soc.* **2013**, *135* (38), 14380–14389.

(31) Muckel, F.; Yang, J.; Lorenz, S.; Baek, W.; Chang, H.; Hyeon, T.; Bacher, G.; Fainblat, R. *ACS Nano* **2016**, *10* (7), 7135–7141.

(32) Fainblat, R.; Frohleiks, J.; Muckel, F.; Yu, J. H.; Yang, J.; Hyeon, T.; Bacher, G. *Nano Lett.* **2012**, *12* (10), 5311–5317.

(33) Delikanli, S.; Akgul, M. Z.; Murphy, J. R.; Barman, B.; Tsai, Y.; Scrace, T.; Zhang, P.; Bozok, B.; Hernández-Martínez, P. L.; Christodoulides, J.; Cartwright, A. N.; Petrou, A.; Demir, H. V. *ACS Nano* **2015**, *9* (12), 12473–12479.

(34) Murphy, J. R.; Delikanli, S.; Scrace, T.; Zhang, P.; Norden, T.; Thomay, T.; Cartwright, A. N.; Demir, H. V.; Petrou, A. *Appl. Phys. Lett.* **2016**, *108* (24), 242406.

(35) Bussian, D. A.; Crooker, S. A.; Yin, M.; Brynda, M.; Efros, A. L.; Klimov, V. I. *Nat. Mater.* **2009**, *8* (1), 35–40.

(36) Fainblat, R.; Muckel, F.; Barrows, C. J.; Vlaskin, V. A.; Gamelin, D. R.; Bacher, G. *ACS Nano* **2014**, *8* (12), 12669–12675.

(37) Piepho, S. B.; Schatz, P. N. *Group theory in spectroscopy: with applications to magnetic circular dichroism*; Wiley-Interscience monographs in chemical physics; Wiley: New York, 1983.

(38) Liu, Y.-H.; Wayman, V. L.; Gibbons, P. C.; Loomis, R. A.; Buhro, W. E. *Nano Lett.* **2010**, *10* (1), 352–357.

(39) Waslela, A.; Peyia, P.; d'Aublgne, Y. M.; Nicholls, J. E.; Ashenford, D. E.; Lunn, B. *Semicond. Sci. Technol.* **1992**, *7* (4), 571–577.

(40) Arciszewska, M.; Nawrocki, M. *J. Phys. Chem. Solids* **1986**, *47* (3), 309–314.

(41) Twardowski, A.; Pokita, E.; Gaj, J. A. *Solid State Commun.* **1980**, *36* (11), 927–930.

(42) Twardowski, A.; Dietl, T.; Demianiuk, M. *Solid State Commun.* **1983**, *48* (10), 845–848.

(43) Gaj, J. A.; Ginter, J.; Gałązka, R. R. *Phys. Status Solidi* **1978**, *89* (2), 655–662.

(44) Twardowski, A.; Swiderski, P.; von Ortenberg, M.; Pauthenet, R. *Solid State Commun.* **1984**, *50* (6), 509–513.

(45) Aggarwal, R. L.; Jasperson, S. N.; Stankiewicz, J.; Shapira, Y.; Foner, S.; Khazai, B.; Wold, A. *Phys. Rev. B* **1983**, *28* (12), 6907–6913.

(46) Yu, W. Y.; Twardowski, A.; Fu, L. P.; Petrou, A.; Jonker, B. T. *Phys. Rev. B* **1995**, *51* (15), 9722–9727.

(47) Hofmann, D. M.; Oettinger, K.; Efros, A. L.; Meyer, B. K. *Phys. Rev. B* **1997**, *55* (15), 9924–9928.

(48) Kuno, M.; Nirmal, M.; Bawendi, M. G.; Efros, A.; Rosen, M. *J. Chem. Phys.* **1998**, *108* (10), 4242.

(49) Taguchi, S.; Ishizumi, A.; Tayagaki, T.; Kanemitsu, Y. *Appl. Phys. Lett.* **2009**, *94* (17), 173101.

(50) Furdyna, J. K. *J. Appl. Phys.* **1988**, *64* (4), R29–R64.

(51) Carter, W. S. *Proc. Phys. Soc.* **1960**, *76* (6), 969–978.

(52) Demper, M.; Heimbrodt, W.; Bradford, C.; Prior, K. A. *J. Nanoparticle Res.* **2011**, *13*

(11), 5635–5640.